Applied Thermal Engineering 110 (2017) 1578–1588

Contents lists available at ScienceDirect

Applied Thermal Engineering

journal homepage: www.elsevier.com/locate/apthermeng

Research Paper

Thermal design of helium cooled divertor for reliable operation

Namkyu Lee [a], Beom Seok Kim [b], Taehwan Kim [a], Ji-Yeul Bae [a], Hyung Hee Cho [a,*]

[a] Department of Mechanical Engineering, Yonsei University, 50 Yonsei-ro, Seodaemun-gu, Seoul 120-749, Republic of Korea
[b] IFW Dresden, P.O. Box 270116, 01171 Dresden, Germany

ARTICLE INFO

Article history:
Received 23 June 2016
Revised 9 September 2016
Accepted 12 September 2016
Available online 12 September 2016

Keywords:
Thermal design
Divertor
Nuclear fusion
Heat transfer
Thermal stress

ABSTRACT

Nuclear fusion is the promising energy sources because the fuels for power generation are abundant and by-products are eco-friendly rather than other power generations. However, there are several conundrums that must be solved for developing the nuclear fusion plants, including DEMO (DEMOnstration nuclear fusion reactors), such as superconducting system, blanket, cryostats and others. In particular, a divertor is one of essential components because of withstanding the excessive heat flux (~10 MW/m^2) from the high-temperature plasma. Therefore, it is necessary for thermal design of divertor module under tremendous heat flux to develop the nuclear fusion plants. We investigate thermophysical behavior by convective heat transfer and suggest principle operating variables to decide for appropriate thermal design for divertor module. Based on the simplified thermal circuit, we demonstrate that the observed correlation can predict thermophysical characteristics of the divertor module and present the prerequisites for reliable thermal design based on the thermal design maps in terms of principle operating variables of divertor module. Finally, we reveal that the safety factor of thimble is primary concern to establish thermal design of divertor module. The present study will contribute to the development of divertor in nuclear fusion plants and the applications for high heat flux and temperature devices.

1. Introduction

Developing sustainable energy sources is a worldwide issue due to definite energy sources and environmental problems. The energy provided by nuclear fusion is one of the most prominent solutions because of its infinite energy source from sea water and ultra-high cost-effective power generation [1,2]. For these reasons, constitutive group called by ITER (International Thermonuclear Experimental Reactor) with seven countries has researched since 2006. However, there are a number of conundrums regarding its engineering feasibility, which include controlling the instability of plasma [3], constructing superconducting systems to confine the plasma [4], irradiation effect on material [5–7], and ensuring the thermal and mechanical characteristics of plasma-facing material [1,8–11]. In particular, a divertor in Fig. 1(a) is one of conundrums to materialize the nuclear fusion plant. The divertor has an essential role in the nuclear fusion plant for maintaining the plasma isolation and plasma purity removing the alpha particles, particle ash, etc. In addition, the H-mode plasma for a step to establish the nuclear fusion plant can be realized by the divertor part in the tokamak [1,12]. However, the divertor should endure the high heat fluxes (~10 MW/m^2) from the plasma during operation, since the divertor is in direct contact with the plasma [1,2]. Therefore, we must acquire an appropriate thermal design that can dissipate the great amount of thermal load from the high temperature plasma.

For the thermal design of divertor module, we should consider the essential requirements that not only guarantee sufficient heat flux removal with high heat transfer efficiency but also ensure uniform temperature distribution to prevent thermal failure of the divertor modules. Conventional thermal design for treating the high thermal load, which are based on convectional heat transfer using functional structures such as rib turbulators [13–16], dimple-protrusions [17–20], pin-fins [21–24], and their integrations [25–28], have been studied to enhance heat transfer performance. Among the various conventional cooling schemes, multiple array impingement jet (MAIJ) cooling is one of the most promising techniques that meet these requirements. MAIJ cooling can guarantee high convective heat transfer coefficients with considerable heat transfer uniformity. As such, it has been widely studied for the design of various heat transfer systems including

* Corresponding author.
E-mail addresses: motivebuzz@yonsei.ac.kr (N. Lee), b.s.kim@ifw-dresden.de (B.S. Kim), kimth0610@yonsei.ac.kr (T. Kim), jyb1988@yonsei.ac.kr (J.-Y. Bae), hhcho@yonsei.ac.kr (H.H. Cho).

http://dx.doi.org/10.1016/j.applthermaleng.2016.09.062
1359-4311/

Nomenclature

a, b, c	correlation coefficient for thermo-hydraulic analysis (°C)
a′, b′, c′	correlation coefficient for thermo-mechanical analysis (MPa)
A	heat transfer area (m^2)
E	elastic modulus
h	heat transfer coefficient (W/m^2 °C)
k	thermal conductivity (W/m °C)
L	length (m)
m, n	exponent constant
$\dot{m}$	mass flow rate (kg/s)
Nu	Nusselt number
p	pressure (Pa)
Pr	Prandtl number
Q	heat flow (W)
Re	Reynolds number
T	temperature (°C)
U	internal energy (J)
v	velocity (m/s)
Y	analogy constant

Greek letter

α	thermal expansion coefficient (1/K)
β	constant value
μ	dynamic viscosity (kg/m s)
ρ	density (kg/m^3)
σ	mechanical stress (Pa)

Subscripts

f	fluid
jet	impingement jet
point	specific location
s	solid

Superscript

∗	non-dimensional sign

gas turbines [29–31], integrated electronic devices [32–34], and various applications [35–38]. It is evident that MAIJ cooling can efficiently dissipate a considerable heat flux, and is also favorable for guaranteeing the thermal stability and uniformity characteristics on a target surface. Based on the merits of powerful and efficient MAIJ cooling, this cooling technique has also been applied to the thermal design of divertor modules.

By experimental and numerical approaches, researchers have proven the adjustable cooling performance of MAIJ with helium in terms of the incident heat flux, mass flow rate, and inlet pressure [8,39,40]. Helium, contrary to water, was chosen as the working fluid for the divertor module with MAIJ cooling because it is not only chemically and neutronically inert and also has high thermal conductivity to increase the heat transfer coefficient regardless of large pressure drop with the change of inlet pressure. For these reasons, researchers have also conducted thermo-hydraulic and thermo-mechanical analyses and have suggested the effects of thermo-hydraulic reliability based on the maximum thimble temperature with the change of incident heat flux and mass flow rate [41–44]. However, with regards to the previous studies of divertor modules with MAIJ cooling, only a limited number of studies have been conducted in terms of the reliable operating ranges. Since the operating variables, which are the mass flow rate and inlet temperature of the working fluid, can be instantaneously changed by the external conditions caused by pulsating or blockages, a universal design guideline and operating domain, which is based on the analytical approach for reliable operation, should be suggested by compensating for the discrete characterizations that are conducted on a confined operating point. Furthermore, evaluation of the mechanical reliability has not been performed during the thermal design of divertor modules. In this sense, the comprehensive evaluation of the divertor module for reliable operation with simplified heat transfer phenomena should be investigated on both operating variables (mass flow rate and inlet temperature) with respect to the satisfied margin for reliable operation.

We suggest the thermal design guideline that considers the thermophysical and mechanical characteristics of the unit cell of the divertor module for reliable operation. Through numerical and analytical approaches, we evaluate the thermo-hydraulic and thermo-mechanical characteristics by convectional cooling and derive the principle variables within the operating domain based on the simplified condition. For establishing the reliable operating domain, a correlated model simplified by a thermal circuit is adopted to physically characterize the fluidic behavior of the working fluid and the consequent heat transfer performance, which involves the maximum thimble temperature and safety factor. From the results of this study, we expected a continuous and expandable thermal design approach for the divertor module. Furthermore, the demonstrations of thermal design presented in this study will useful in the thermal design of divertor components in nuclear fusion plants and for extending their applications for high heat flux and temperature devices.

2. Methodology

2.1. Structural design and variables: Unit cell of a divertor system with multiple array impinging jets

Fig. 1(b) and (c) denotes a module and a unit cell of the divertor module. A divertor module consists of hexagonally-arranged unit cells with a width of 17.8 mm where the total number of unit cells covering the divertor is 0.5 million [45]. The center hole diameter, which is single hole at the center of cartridge, is 1.0 mm and other holes is 0.6 mm, 24 holes around the center hole. The hole arrangement is 5 array included center hole and hexa-staggered arrangement from the center hole. The fluid path between jet hole and target surface of thimble is 0.9 mm. The unit cell is composed of a tile, thimble, and cartridge. The tile, which directly contacts the plasma and is exposed to extremely high heat flux conditions, is tungsten and has a melting temperature of 3422 °C and a thermal conductivity ranging from 101 W/m °C to 173 W/m °C in the operating range [1]. The thimble (WL10), with a thermal expansion coefficient of 4.6 μm/m °C, is inserted between the tile and the cartridge (ODS (Oxide dispersion-strengthened alloy) steel) to compensate for the significant difference of the thermal expansion coefficients of the tile (4.0 μm/m °C) and the cartridge (10.4 μm/m °C) at $T = 20$ °C [1]. The tile is bonded with the thimble, and the cartridge is connected with the main channel of the working fluid (helium). The working fluid is vented through multiple jet-holes of the cartridge towards the thimble and dissipates the thermal loads through a fluidic channel between the thimble and the cartridge. The factors of the mass flow rate and inlet temperature of the helium are the two principle design variables; the thermo-hydraulic performance of the divertor component is clearly governed by these factors [1,41].

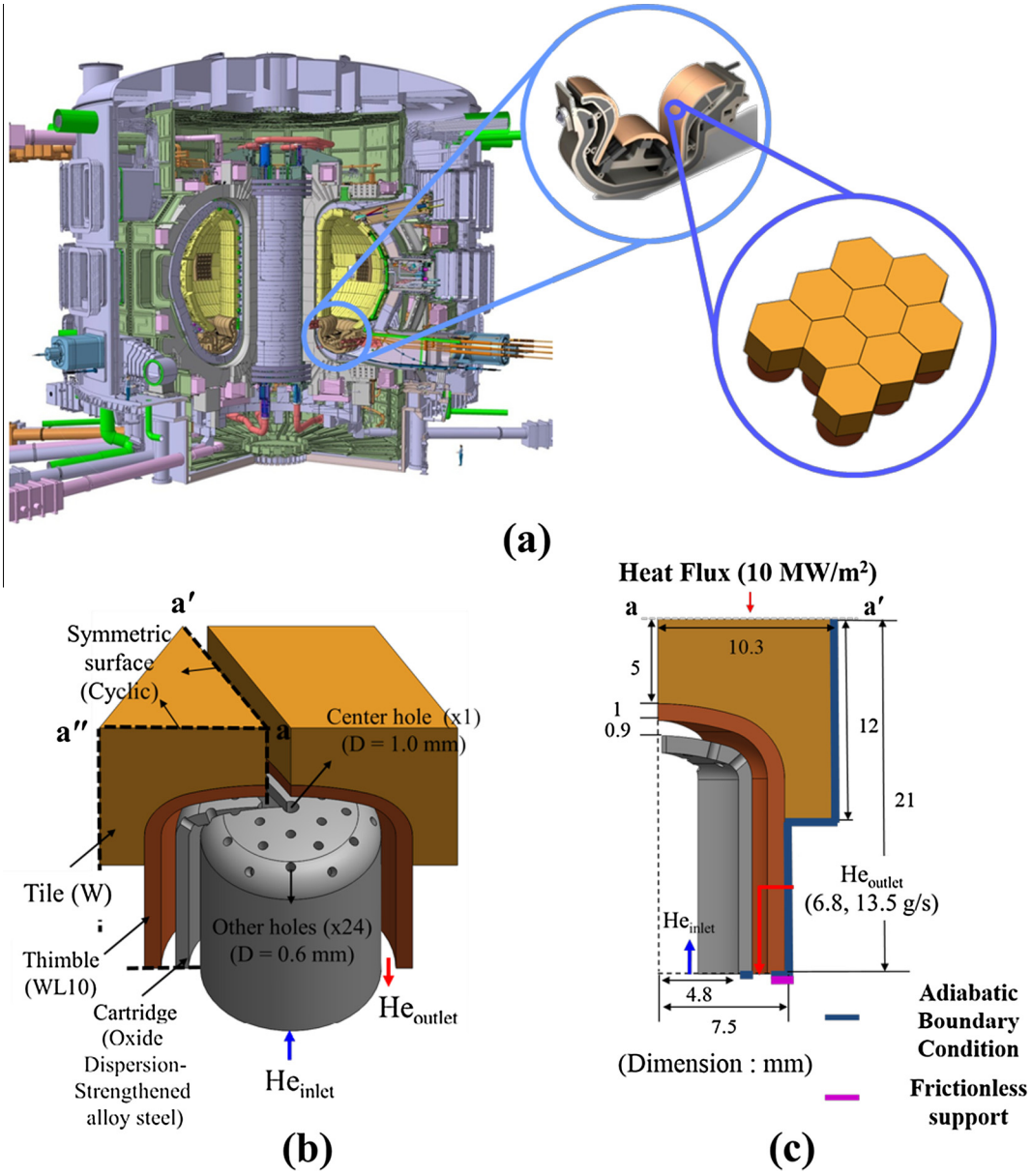

Fig. 1. Schematic of (a) divertor section in the Tokamak (Copyright from ITER Organization) [2], (b) and (c) the divertor module with MAIJ (multi array impingement jet) cooling included in the boundary conditions and geometrical information of computational fluid dynamics and mechanical analysis.

2.2. Analysis of fluidic and heat transfer performance

2.2.1. Modeling of thermo-hydraulic and thermo-mechanical analysis

To evaluate the convective effects by the impinging jets of helium on a divertor unit cell, the physical behaviors of the fluid can be described using governing equations that explain the balance of continuity, momentum, and energy. The equations under a steady state condition can be expressed as follows [46]:

$$\nabla \cdot (\rho \vec{v}) = 0 \tag{1}$$

$$\vec{v}(\nabla \cdot \vec{v}) = -\nabla\left(\frac{p}{\rho}\right) + (\mu + \mu_t)\nabla^2 \vec{v} \tag{2}$$

$$\rho(\vec{v} \cdot \nabla U) - \nabla \cdot (k\nabla T) + p\nabla \cdot \vec{v} = 0 \tag{3}$$

where ρ, $\vec{v}$, p, μ, μ_t, U, k, and T are the helium density, velocity, pressure, dynamic viscosity, turbulent viscosity, internal energy, thermal conductivity, and temperature, respectively. A commercial code, CFX 15.0, is used to discretize and solve the equations to characterize thermo-hydraulic characteristics of the unit cell. The Reynolds-averaged Navier-Stokes (RANS) equations are reflective of turbulent quantities. We choose the shear stress transport (SST) model to calculate the turbulent viscosity quantitatively based on the past research [47]. In the past research, k-ε model cannot

Table 1
Variables for the cases in this study.

Case	Operating variables	
	Mass flow rate (g/s)	Inlet temperature (°C)
1	6.8	540
2	6.8	587
3	6.8	634
4	13.5	540
5	13.5	587
6	13.5	634

Table 2
Properties of the solid materials in this study.

	Density (kg/m^3)	Specific heat (J/kg °C)	Thermal conductivity (W/m °C)	Elastic modulus (GPa)/thermal expansion coefficient (μm/m °C)
Solid (T = T [°C])				
Tungsten (W)	19,000	$C_p(T) = 119.0 + 3.530E-2*T-3.667E-6*T^2$	$k(T) = 174.9-0.107*T+5.007E-5*T^2-7.835E-9*T^3$	398/4.0 at 20 °C 390/4.2 at 500 °C 368/4.5 at 1000 °C 333/4.8 at 1500 °C
Tungsten-alloy (WL10)	19,000	$C_p(T) = 107.4 + 7.176E-2*T-2.823E-5*T^2$	$k(T) = 124.3-4.148E-2*T+1.443E-5*T^2$	398/4.6 at 20 °C 390/4.8 at 500 °C 368/5.0 at 1000 °C 333/5.1 at 1500 °C
ODS (Steel)	7680	$C_p(T) = 406.1 + 3.455E-2*T+4.152E-4*T^2$	$k(T) = 19.37 + 2.816E-2*T-2.025E-5*T^2$	–

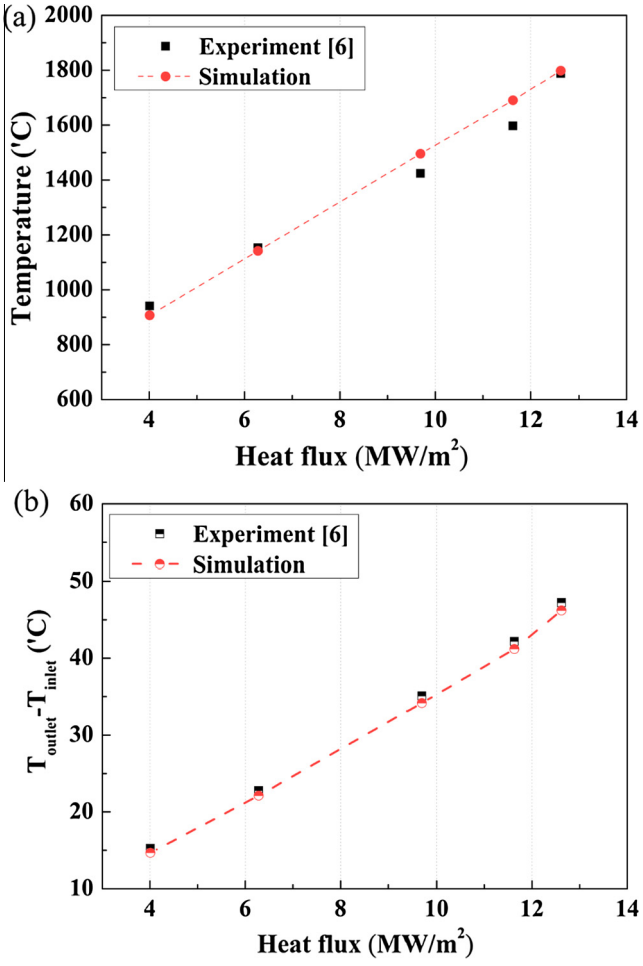

Fig. 2. Comparison reported experimental results with simulation results: (a) maximum temperature of divertor module and (b) temperature difference of helium coolant at inlet and outlet.

estimate the fluid characteristics near the wall because of poor approximation and RNG k-ε predict the larger jet-spreading rates compared to the experiments. On the other hand, the SST model can predict thermal and fluidic phenomena compared to other turbulent model. Thus, SST model is applied to the study for estimation of impingement jet cooling behavior in the divertor module [47]. Additionally, a high resolution scheme is used for capturing variation in the fine grids.

The thermal stress, which is caused by local and overall heat transfer characteristics, is evaluated to demonstrate the thermal

Table 3
Known parameters in Eq. (5).

Known parameters	
q″ (Q/A)	10 MW/m^2
$T_{f,\ jet}$	540, 587 and 634 °C

failure of the system. The thermal stress is obtained from the pre-process of the heat transfer evaluations and can be analytically explained as follows:

$$\sigma_{thermal\ stress} = E\alpha\Delta T_s \quad (4)$$

where E, α, and T_s indicate the Young's modulus of the solid, thermal expansion coefficient, and consequent temperature of the solid components from the analyses of fluidics and heat transfer, respectively. The equivalent stress (i.e., von Mises stress), which represents the status of the yield condition, is obtained from an additional analysis process based on the finite element method using ANSYS Mechanical Products 15.0.

In the designated operating domain, the detailed inlet conditions of these variables are presented in Table 1 (at a constant pressure of 10 MPa) to consider the operating domain of divertor module [1,41]. We assess the mechanical reliability for a unit cell as a function of the thermal stress. The geometry is a one-sixth segment, as represented in Fig. 1(b), but the cartridge is excluded in the mechanical analysis because it has a small temperature gradient and does not link with the tile and thimble structure. The cut surfaces along with a-a′ and a-a″ are symmetric surfaces in CFD (Computational Fluid Dynamics) and cyclic surfaces in the mechanical analysis. The bottom surface of the thimble is considered to be frictionless support condition [1] and the other parts are exposed to free thermal expansion. As shown in Fig. 1(c), reflecting the thermal load from the plasma, a constant heat flux of 10 MW/m^2 is loaded to the upper surface of the tile, and adiabatic conditions are set at the outer component. The temperature and pressure distribution for the boundary condition in the mechanical analysis originate from the CFD result. For reasonable demonstration of the thermal stress, all thermo-physical intrinsic properties are simulated as a function of temperature [1] (see Table 2).

2.2.2. Grid formation and validation

For the computational fluid dynamics, unstructured meshes with more than 6.6 million components are used by ANSYS to minimize the analytical uncertainty and grid dependency. To accurately evaluate the fluidic and consequent heat transfer characteristics, meshes are densely generated near the solid-fluid interfaces between the thimble and the working fluid. In particular, the wall y-plus value is adjusted to be less than 1 due to the

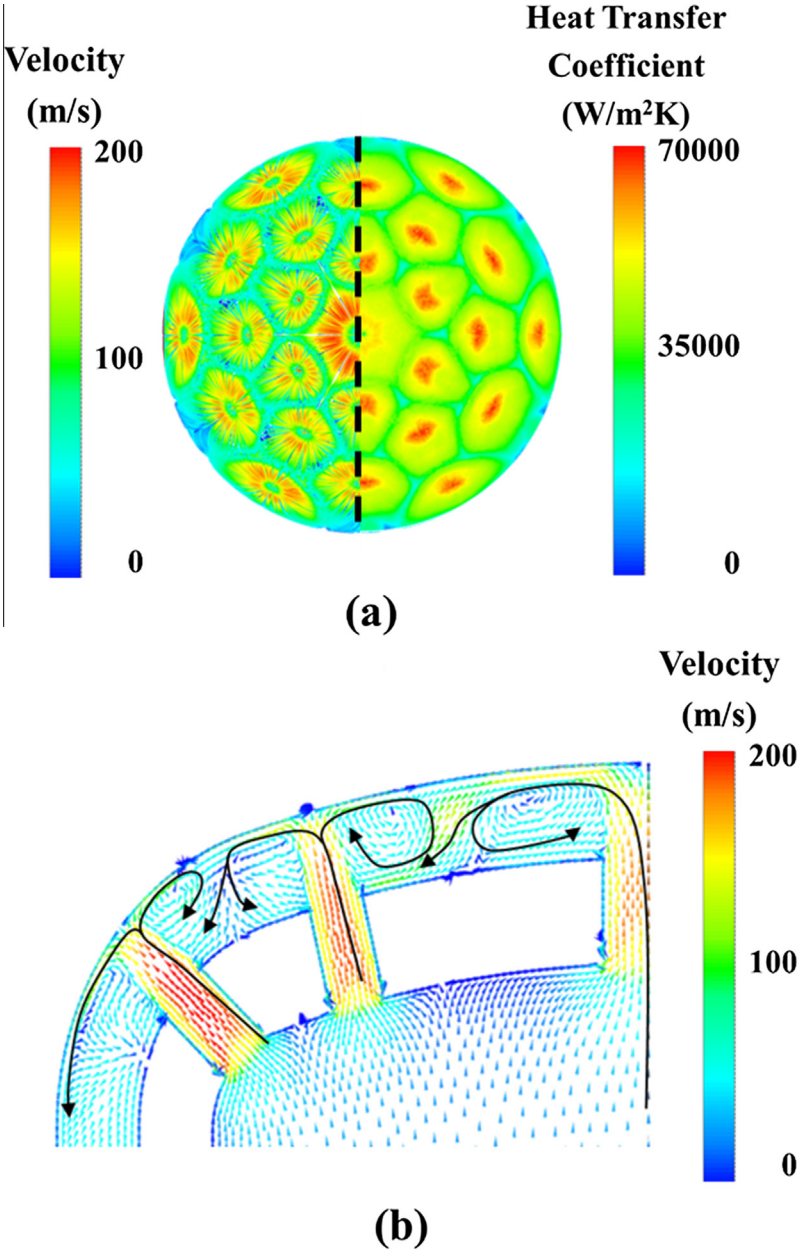

Fig. 3. Simulation results in Case 1 ($\dot{m} = 6.8$ g/s. $T_{inlet} = 540$ °C): (a) Streakline through the flow path and heat transfer coefficient on the surface, (b) velocity field at mid-span in the divertor.

importance that the first grid point from the wall accurately estimates the heat transfer characteristics [48]. The numerical reliability is validated by comparison with the reported experimental results, which correspond to the operating domains of the variables in Fig. 2 [41,48,49]. The discrepancy of numerical simulation results with reported experimental results is within 5.9% of the maximum temperature of divertor module and 3.8% of the difference between helium inlet and outlet temperature, which is sufficient for the numerical reliability of the research. The grid for the thermo-mechanical analysis is generated by ANSYS and the total number of grid components is about 0.5 million in order to satisfy grid independency.

2.3. Analytical approach by thermal circuit

For a model for evaluating thermal design of divertor module, we need to simplify the sophisticated heat transfer phenomena. Assuming that the divertor module is treated as a simple lump body exposed to a constant heat flux and that the conductive heat loss is negligible, a one-dimensional thermal circuit can be used to determine the temperature with the operating variables. Through a one-dimensional thermal circuit, the local temperature in the unit cell can be expressed by the following relation:

$$\Delta T = T_{local} - T_{f,jet} = Q\left(\frac{L_{tile}}{k_{tile}A} + \frac{L_{thimble}}{k_{thimble}A} + \frac{1}{h_{jet}A}\right) = q''\left(\frac{L_{tile}}{k_{tile}A} + \frac{L_{thimble}}{k_{thimble}A} + \frac{1}{h_{jet}A}\right) \quad (5)$$

where T_{local}, $T_{f,jet}$, Q, A, and h_{jet} are the local temperature in the divertor, inlet temperature of the jet flow, heat flow, unit area, and heat transfer coefficient by the jet flow, respectively. The known parameters are arranged in Table 3. $L_{thimble}$ and L_{tile} (i.e. the heat flow path length) are defined as the penetrated distance through thimble and tile by heat flow in the path from the upper

side of tile to working fluid to dissipate the heat flow. In Eq. (5), Q and A are constant because we assumed that one-dimensional thermal conduction without conductive loss. If the thermal conductivity of tile (tungsten) and thimble (WL 10) is constant, we changed Eq. (5) to following Eqs. (6) and (7) as follows:

$$T_{local} = T_{f,jet} + QR_{cond.tile} + QR_{cond.thimble} + QR_{conv.} = T_{f,jet} + QR_{conv.} + Const. \quad (6)$$

$$R_{cond.} = \frac{L}{kA},\ R_{conv.} = \frac{1}{h_{jet}A} \quad (7)$$

From the assumption which is Q, A and k of tile and thimble is constant within operating ranges, we can gather Eq. (6) which is a function of $T_{f,jet}$ and h_{jet}. In next, h_{jet} in Eq. (7) is expressed by the Nusselt number, the Reynolds number and the Prandtl number for the conversion from heat transfer coefficient to mass flow rate as follows [50]:

$$Nu = \frac{h_{jet}D}{k_f} = YRe^m Pr^n \quad (8)$$

$$h_{jet} = Y\frac{k_f}{D}\left(\frac{\dot{m}}{\mu\frac{\pi}{4}D}\right)^m (Pr)^n = \beta(\dot{m})^m \quad (9)$$

where k_f, $\dot{m}$, D, Y, β, and m are the thermal conductivity of the fluid, mass flow rate, jet diameter, analogy constant, empirical constant, and exponent, respectively. The exponent constant of m is 0.8 in the case of array impingement jet cooling on a flat plate, as presented in a previous experimental study [51]. In the operating temperature range, Pr and D are constant and k_f/μ^m at the inlet varies by 1.6% in all cases. Thus, we can assume that β is a constant value in this study. Herein, we use two normalized factors for the temperature ($T^* = (T_{f,in} - 540)/(634 - 540)$) and mass flow rate ($\dot{m}^* = \dot{m}/13.5$), which consider the domain of the two variables presented in Table 1. By substitution of the terms in Eqs. (6) and (9), we can derive an intuitive relation between the operating variables and the consequent local temperature as follows:

$$T_{local} = aT^* + b(\dot{m}^*)^{-0.8} + c = f(T^*, \dot{m}^*) \quad (10)$$

where a, b, and c are the correlating coefficients associating the thermo-hydraulic results. a represents the temperature variation depending on the inlet temperature at a specific point, b is a function of β (an empirical constant) and heat flow, and c accounts for the thermal resistance of the tile and thimble. Based on the analytically-simplified model expressed by Eq. (10), it is evident that the local temperature in the divertor module can be quantitatively determined as a function of the two principle operating variables.

3. Results and discussions

3.1. Effects of impinging jet on local/overall heat transfer and the maximum thimble temperature

To evaluate the reliability of the divertor, we first evaluate the local heat transfer performance induced by the impinging jet flow. Fig. 3(a) and (b) shows the local heat transfer coefficients (HTCs) with streaklines through the flow path and cross sectional velocity field of case 1 ($\dot{m} = 6.8$ g/s, $T_{inlet} = 540\,^{\circ}$C) in Table 1, when a helium jet impinges on the thimble. The results show that HTC is dominated on the stagnation region. As the helium stream is supplied with a high Reynolds number (>20,000) in the turbulent regime, the stream jets are accelerated via the jet holes of the cartridge. The accelerated jets then impinge on the thimble surface and interact in a downward direction with a cross flow formed by spent gas of upstream jets, generating local counter vortices. In addition, working fluid from jet hole accelerates toward the downstream and meets with shear layer from jet, which enhances the heat transfer phenomena at the stagnation region. Additionally, high heat transfer coefficient spreads toward downstream due to the crossflow and hole arrangement. We can see that the local impinging jets are essential for convective heat dissipation against the high heat flux with an accelerated local velocity above 180 and 200 m/s at the center and side holes in Fig. 3(a) and (b), respectively. Finally, the effects of local impinging jets and the consequent cross flow characterize the overall heat transfer performance according to variations in the inlet velocity and temperature of the helium. Fig. 4 presents the temperature distribution along the tile and thimble surfaces. The applied heat flux starts to be conducted from the top to the bottom of the tile, while the convective heat dissipation occurs at the flow passage between the

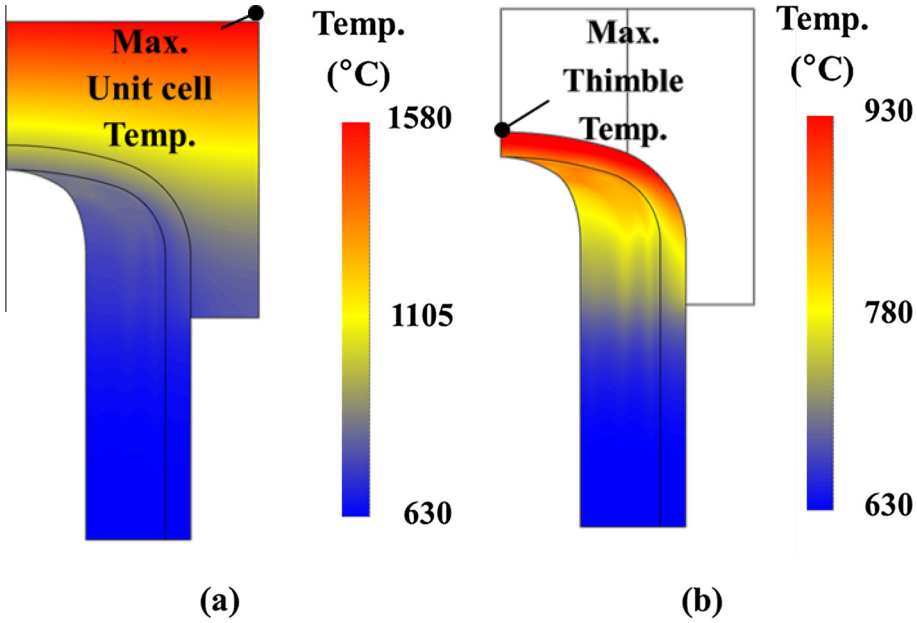

Fig. 4. Temperature distribution of the divertor unit cell in Case 1 ($\dot{m} = 6.8$ g/s. $T_{inlet} = 540\,^{\circ}$C): (a) Divertor module, (b) Thimble.

thimble and cartridge. The thermal load is consequently concentrated at the edge of the tile due to the longest path length of the thermal conduction through the tile. This explains why the maximum local temperature shown in Fig. 4 occurs at the top-edge of the tile. The maximum temperature of the thimble is observed at the center of the component because the thermal resistance is the lowest between the top of the tile and the thimble along the vertical direction. However, the quantitative local temperature distributions are clearly dependent on the inlet conditions of the helium temperature and mass flow rate with Eq. (10). Increase in the helium temperature and mass flow rate lead to increase and decrease in the overall temperature of the components, respectively. The local thermal characteristics of the divertor are purely governed by the convective cooling associated with the impinging jets. It can be demonstrated that effective cooling and heat dissipation can be achieved by enhancing the degree of subcooling and by increasing the capacity of the coolant.

The operating temperatures should be determined by the intrinsic melting temperatures of the devices. Therefore, in all cases, the maximum temperature of the module should not exceed 1683 °C. This is much less than the allowable temperature of tungsten (2300 °C) [52]. Intuitively, we can allow the operating conditions of the coolant to prevent thermal failure of the tile against excessive thermal load. However, the brazing temperature of STEMET® (~1050 °C), which is typically used to assemble the divertor module, must be considered as an additional criterion for determining the operating conditions [41,53]. Fig. 5 indicates the maximum temperature of the thimble and correlated curves, which predict the temperature according to the operating variables in the domain. The correlation coefficients are extracted from the analytical results of the thermo-hydraulic characteristics. *a*, *b*, and *c* in Eq. (10) are determined to be 83.41, 71.31, and 879.0, respectively. The correlations expressed by Eq. (10), using the three correlation factors, agree well with the numerical simulation results and are within ±0.5% for the entire operating domain. However, in Fig. 5, we can see that the maximum temperature of the thimble, which ranges from 945.0 °C to 1079 °C, varies according to the inlet conditions; this range partially exceeds the brazing temperature of STEMET® (T‴). Therefore, we must confine the allowed operating domain of the inlet conditions in order to ensure that the brazing temperature is not exceeded.

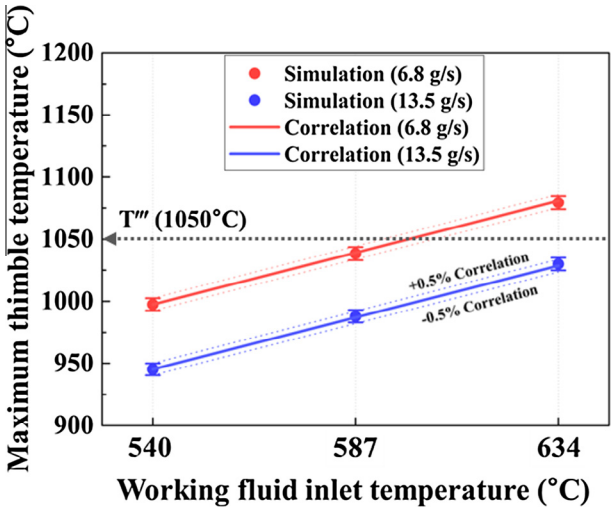

Fig. 5. Comparison between the numerical simulation results and the correlation results for the maximum thimble temperature (T‴ (1050 °C): STEMET® brazing temperature).

3.2. Thermo-mechanical characteristics of unit cell for assessment of reliability

The thermal stress must be retained below the yield strength because the mechanical properties of materials above the yield strength are vulnerable in the plastic region and are fragile under mechanical stresses. Harsh thermal environments accompanying high temperatures and the presence of a significant temperature gradient induce high thermal stresses and/or low yield strengths. Thus, characterizing the system in terms of the thermally-induced stress is also essential for determining the thermo-mechanical reliability. Fig. 6 presents the estimated results of the equivalent (Von-Mises) stress distribution of the tile and thimble. We can see that the center in the upper part of the tile has weaknesses in its thermal stress because the high temperature, especially at a heat flux entering the surface, results in a scenario where the yield strength is surpassed. Alternatively, the curved area in the thimble is susceptible to thermal stress because the curved part is exposed to the maximum strain by thermal expansion in the unit cell. The quantitative values of thermal stress at these vulnerable points are presented in Fig. 7. The temperature of tile and thimble has agreeable margin at these vulnerable points compared to the temperature limits of tungsten and WL10 [34,45].

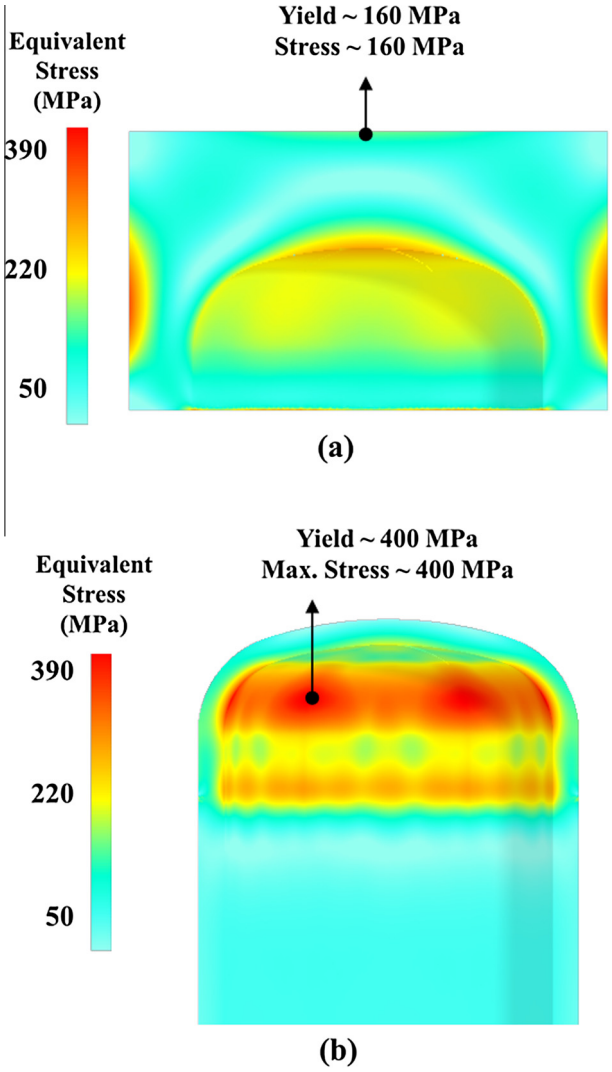

Fig. 6. Equivalent stress (Von-Mises stress) distribution at the divertor unit cell in Case 1 ($\dot{m} = 6.8$ g/s. $T_{inlet} = 540$ °C): (a) Tile, (b) Thimble.

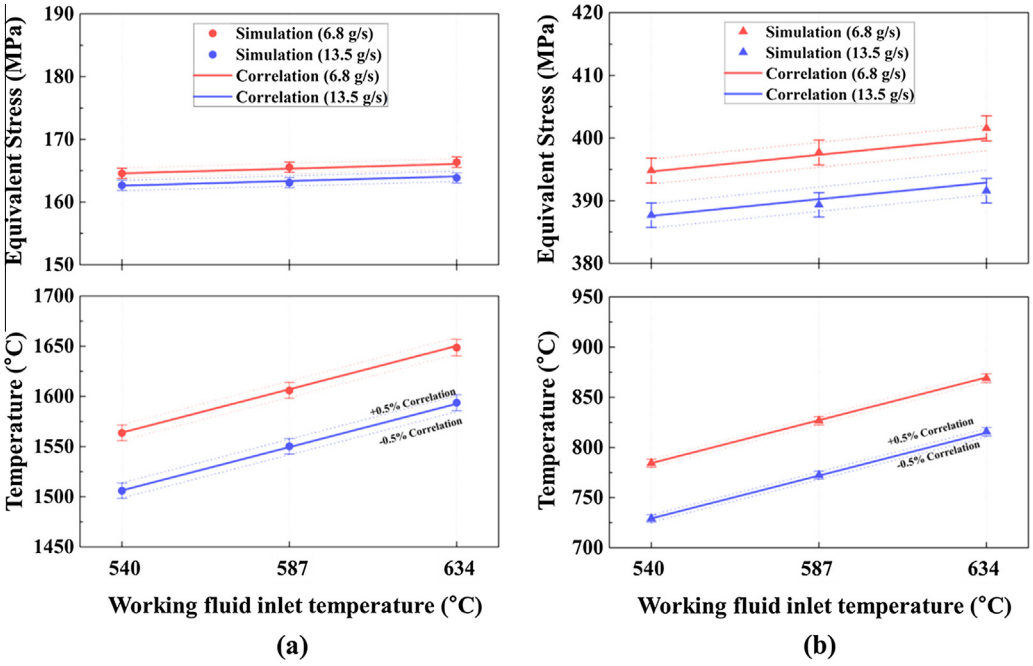

Fig. 7. Comparison between the numerical simulation results and correlation results for the equivalent stress and temperature at the vulnerable points: (a) Tile, (b) Thimble.

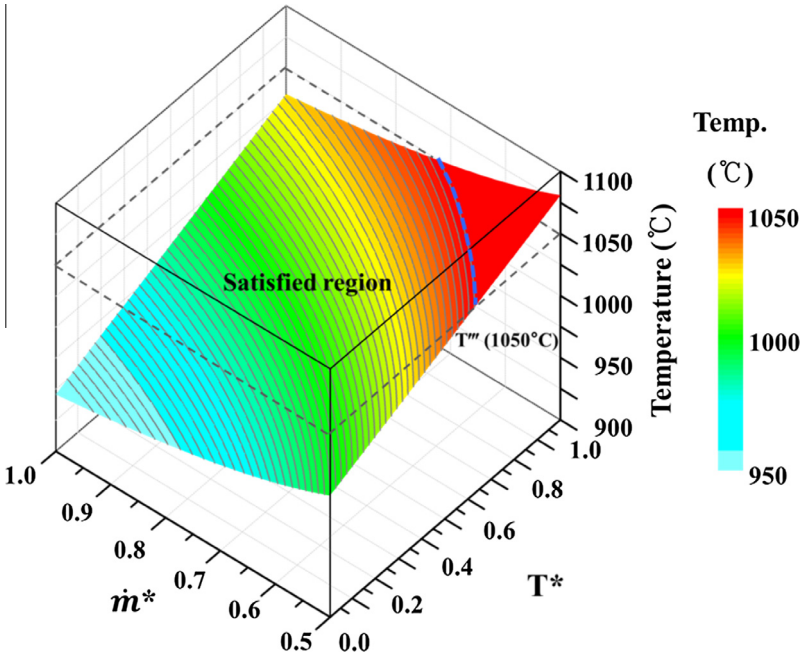

Fig. 8. Thermal design map for the maximum thimble temperature in the operating range (T‴: Baseline of temperature (1050 °C)).

The thermal stress of the tile in the center region ranges from 162.9 to 166.4 MPa (according to the operating variables), and the thermal stress of the thimble ranges from 387.7 to 401.6 MPa. Because the yield strength is a function of the temperature in the Ref. [1], we can presume that the thermal stress approaches the yield strength at the vulnerable portions of the divertor module from temperature, respectively. Thus, we should consider the thermo-mechanical reliability in terms of the thermal stress and yield strength at these specific points.

As shown in Fig. 7, we derive the correlation equation from the numerical simulation results. As the temperature increases, every elements expands toward specific directions based on their crystal structures due to thermal expansion. For this reason, due to thermal expansion, the dimensions of block increases and the thermal strain appears on the elements defined as the multiplication of thermal expansion coefficient and temperature difference. Sequently, as the hooke's law, the thermal stress happen to the elements determined from the multiplication of elastic moduls and thermal strain as shown in Eq. (4) [54]. For these reasons, thermal stress is proportional to the temperature difference and also expressed to the temperature, which is a function of operating variables, at the vulnerable points in the divertor module. Thus,

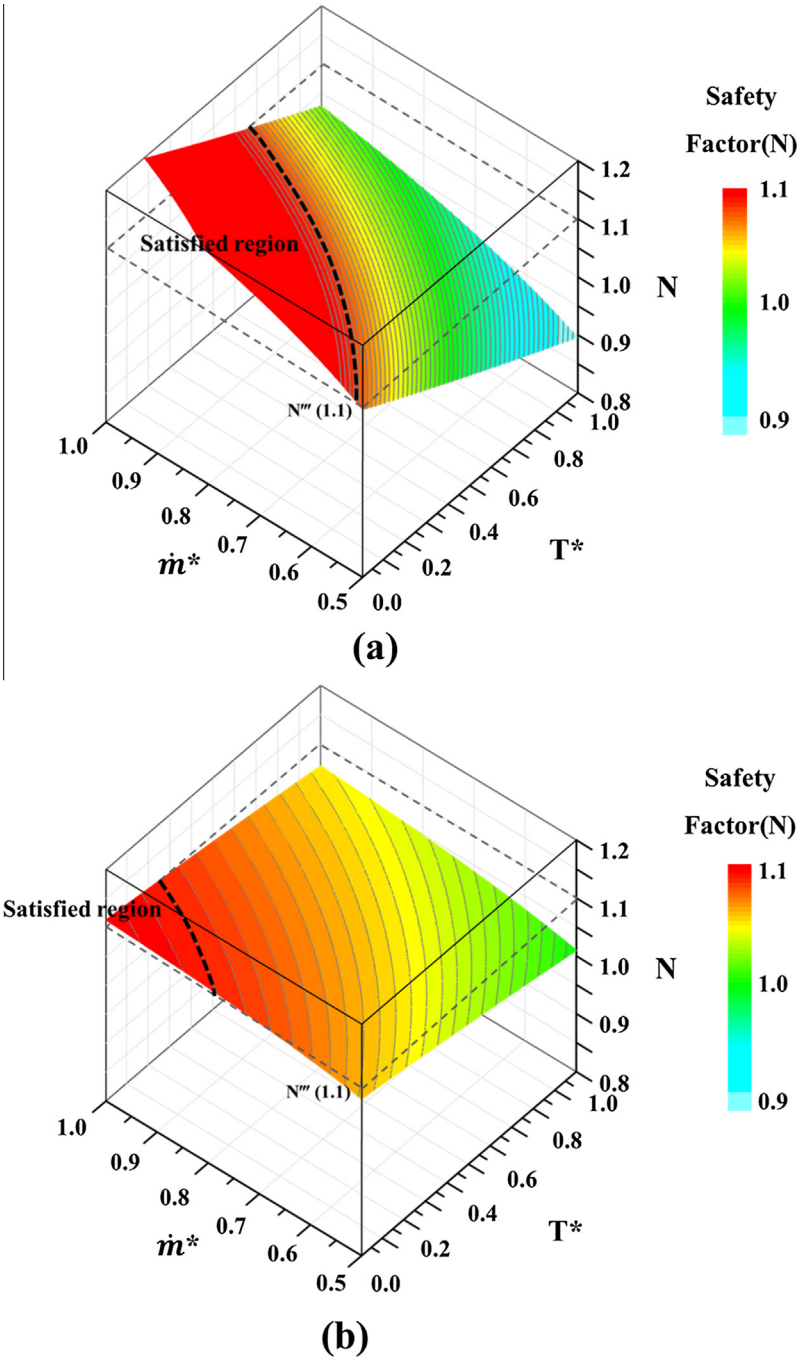

Fig. 9. Thermal design map for the safety factor in the operating range: (a) Tile, (b) Thimble (N‴: Baseline of safety factor (1.1)).

based on Eq. (4), similarly to the thermo-hydraulic analysis, the local stress and temperature for yield strength can be predicted as follows:

$$\sigma_{calculated\ stress} = a'T^* + b'(\dot{m}^*)^{-0.8} + c' \quad (11)$$

$$T'' = AT^* + B(m^*)^{-0.8} + C \quad (12)$$

where a', b', c', A, B, and C are the correlation coefficients related to the stress and temperature covering the operating conditions. Using the numerical simulation results, the correlation coefficients a', b′, and c' involving the local stress predictions are 1.485, 2.702, and 159.9 in the tile and 5.310, 9.683, and 377.9 in the thimble, respectively. A, B, and C are the correlation coefficients for temperature covering the operating conditions. These values are 86.40, 78.58, and 1428 in the tile and 85.58, 75.45, and 653.7 in the thimble, respectively. As shown in Fig. 7(a), the maximum difference between the correlations and numerical calculations for the tile and thimble are 0.17% and 0.39% in the thermal stress over the operating range, respectively. In addition, as presented in Fig. 7 (b), the maximum difference of temperature for yield strength in the tile and thimble are within 0.5% over the operating range. This shows that the correlations of the thermo-mechanical results are sufficient within the operating range.

3.3. Thermal design map for the unit cell of the divertor module

In the process of thermal design, mapping the system reliability is a step that can be utilized to reveal the margin of operating variables within the domain. Since the operating variables can be

determined from the desired power generation performance, and can be considered to vary abruptly due to the harshness of the operating conditions, we should evaluate the reliable region in the operating domain for each demanded requirement. Furthermore, when we optimize the mechanical system, the satisfied region in the thermal design map can provide useful results for determining the system performance [55,56]. Fig. 8 shows that the maximum thimble temperature is dependent on the operating variables, including the non-dimensional mass flow rate ($\dot{m}^*$) and working fluid inlet temperature (T^*), as predicted by Eq. (10). The blue dashed line indicates the thermal design criterion describing the maximum thimble temperature (1050 °C). Fig. 8 also shows that increasing the mass flow rate and decreasing the fluid temperature enhances the thermophysical reliability. We can also determine the satisfied domain in the operating condition using the analytic equations. Based on the blue dashed line, the satisfied fraction in the operating range is about 93%.

Using Eqs. (11) and (12), we can acquire the correlations in terms of the stress and temperature for yield strength. In general, the mechanical reliability is determined from the integrated factors because the mechanical properties have a large difference based on the yield strength. Thus, a safety factor can be instituted in order to present systematic design guidelines by integrating factors such as the yield strength and thermal stress. The safety factor N is expressed as follows:

$$N = \frac{\sigma_{yield}(T^*, \dot{m}^*)}{\sigma_{actual}(T^*, \dot{m}^*)} \tag{13}$$

where both yield strength and actual stress are purely dependent on the operating variables of T^* and $\dot{m}^*$. Fig. 9(a) and (b) shows the safety factor of the tile and thimble, respectively, depending on the operating variables that are determined with Eq. (13). The black dashed line for the design criterion of the safety factor (N‴ (1.1)) in Fig. 9 is determined from the mechanical condition to evaluate the mechanical system [57]. As shown in Fig. 9(a) and (b), the suitable safety factor regions in the tile and thimble are also obtained at the high mass flow rate and low working fluid inlet temperature; in the high heat flux condition, the temperature is one of the key issues related to the simultaneous decrease in the thermal stress and increase in the yield strength. In Fig. 9(a), for the tile, the black dashed line shows that the satisfied portion in the operating range is about 37%. In Fig. 9(b), for the thimble, the black dashed line shows that the satisfied portion in the operating range is about 7.8%. In order to ensure the mechanical reliability of the thimble, the operating variables should be maintained within the limited margin that is made by connecting $T_{f,in}$ of 602.4 °C with $\dot{m}^* = 1.0$ and $\dot{m}$ of 7.09 g/s with the $T^* = 0.0$.

In conclusion, by determining the satisfied portion by using the reliability criteria, we can reveal that the mechanical reliability of the thimble should be a primary consideration for the thermal design of divertor modules based on the principle variables. Using a thermal design map, we can also define the reliable operating range within limited inlet temperature and mass flow rate of the divertor module.

4. Conclusion

To suggest a thermal design guideline for the unit cell of a divertor module in a nuclear fusion reactor, we evaluated the thermophysical behavior based on the numerical simulation and correlated approach for comprehensive understanding in the operating domain. To derive the correlation of the divertor module, we simplified the sophisticated heat transfer phenomena and revealed mass flow rate and inlet temperature of the working fluid (He) to affect the thermophysical behavior of the divertor module. Through thermo-hydraulic analysis, we investigated not only the local/overall heat transfer characteristics but also an essential criterion for the divertor module that reflects the maximum thimble temperature confined by the brazing temperature. In the thermo-mechanical analysis, we indicated the vulnerable spots within the tile and thimble. We introduced the safety factor, which integrates both the equivalent stress and yield strength, was used as a guideline against thermal failure by thermal stress. From the results of thermo-hydraulic and -mechanical analysis, we can derive the thermal design map using the correlation in the operating domain about the maximum thimble temperature and safety factor of the divertor module. Through the deduction of satisfied region in the thermal design map, we recognize that the safety factor of the thimble should be the primary design point for the thermal design of the unit cell. These results should be helpful in establishing the thermal design process of divertor for nuclear fusion plants. In addition, we expected that thermal design process can be helpful for the additional effects, which consists of inlet pressure, neutron, materials, and others, through integrating the components on the analytical and numerical approach. The presented approach, based on correlated and numerical methodology, can also be applied to the optimization of the structural design of various devices and operating conditions within thermo-hydraulic systems.

Acknowledgements

This work was supported by a National Research Foundation of Korea (NRF) grant funded by the Korea government (MEST) (No. 2011-0017673) and the Human Resources Development program (No. 20144030200560) of the Korea Institute of Energy Technology Evaluation and Planning (KETEP) grant funded by the Korea government Ministry of Trade, Industry and Energy.

References

[1] P. Norajitra, Divertor Development for a Future Fusion Power Plant, KIT Scientific Publishing, 2014.
[2] ITER, <http://www.iter.org/>.
[3] T. Hender, J. Wesley, J. Bialek, A. Bondeson, A. Boozer, R. Buttery, et al., MHD stability, operational limits and disruptions, Nucl. Fusion 47 (2007) S128.
[4] E. Doyle, W. Houlberg, Y. Kamada, V. Mukhovatov, T. Osborne, A. Polevoi, et al., Plasma confinement and transport, Nucl. Fusion 47 (2007) S18.
[5] A. Hasegawa, M. Fukuda, K. Yabuuchi, S. Nogami, Neutron irradiation effects on the microstructural development of tungsten and tungsten alloys, J. Nucl. Mater. 471 (2015) 175–183.
[6] E. Materna-Morris, R. Lindau, H.-C. Schneider, A. Möslang, Tensile behavior of EUROFER ODS steel after neutron irradiation up to 16.3 dpa between 250 and 450 °C, Fusion Eng. Des. 98–99 (2015) 2038–2041.
[7] M. Übeyli, Ş. Yalçın, Neutronic study on a magnetic fusion reactor using protective liquid wall of thorium molten salts, Energy Convers. Manage. 49 (2008) 947–952.
[8] P. Norajitra, A. Gervash, R. Giniyatulin, T. Ihli, W. Krauss, R. Kruessmann, et al., He-cooled divertor for DEMO: experimental verification of the conceptual modular design, Fusion Eng. Des. 81 (2006) 341–346.
[9] G. Ritz, T. Hirai, J. Linke, P. Norajitra, R. Giniyatulin, L. Singheiser, Post-examination of helium-cooled tungsten components exposed to DEMO specific cyclic thermal loads, Fusion Eng. Des. 84 (2009) 1623–1627.
[10] P. Norajitra, S. Antusch, L.V. Boccaccini, M. Kuzmic, I. Maione, L. Spatafora, He-cooled demo divertor: design verification testing against mechanical impact loads, Fusion Eng. Des. 87 (2012) 932–934.
[11] S. Kakarantzas, A. Grecos, N. Vlachos, I. Sarris, B. Knaepen, D. Carati, Direct numerical simulation of a heat removal configuration for fusion blankets, Energy Convers. Manage. 48 (2007) 2775–2783.
[12] G. Janeschitz, A. Antipenkov, G. Federici, C. Ibbott, A. Kukushkin, P. Ladd, et al., Divertor design and its integration into ITER, Nucl. Fusion 42 (2002) 14.
[13] J. Han, J.S. Park, Developing heat transfer in rectangular channels with rib turbulators, Int. J. Heat Mass Transfer 31 (1988) 183–195.
[14] K.M. Kim, B.S. Kim, D.H. Lee, H. Moon, H.H. Cho, Optimal design of transverse ribs in tubes for thermal performance enhancement, Energy 35 (2010) 2400–2406.
[15] J. Liu, J. Gao, T. Gao, X. Shi, Heat transfer characteristics in steam-cooled rectangular channels with two opposite rib-roughened walls, Appl. Therm. Eng. 50 (2013) 104–111.
[16] G. Xu, Y. Li, H. Deng, Effect of rib spacing on heat transfer and friction in a rotating two-pass square channel with asymmetrical 90-deg rib turbulators, Appl. Therm. Eng. 80 (2015) 386–395.

[17] H. Moon, T. O'Connell, B. Glezer, Channel height effect on heat transfer and friction in a dimpled passage, J. Eng. Gas Turbines Power-Trans. ASME 122 (2000) 307–313.
[18] S.D. Hwang, H.G. Kwon, H.H. Cho, Local heat transfer and thermal performance on periodically dimple-protrusion patterned walls for compact heat exchangers, Energy 35 (2010) 5357–5364.
[19] C. Bi, G.H. Tang, W.Q. Tao, Heat transfer enhancement in mini-channel heat sinks with dimples and cylindrical grooves, Appl. Therm. Eng. 55 (2013) 121–132.
[20] W. Siddique, N.A. Khan, I. Haq, Analysis of numerical results for two-pass trapezoidal channel with different cooling configurations of trailing edge: the effect of dimples, Appl. Therm. Eng. 89 (2015) 763–771.
[21] R. Goldstein, M. Jabbari, S. Chen, Convective mass transfer and pressure loss characteristics of staggered short pin-fin arrays, Int. J. Heat Mass Transfer 37 (1994) 149–160.
[22] J.S. Park, K.M. Kim, D.H. Lee, H.H. Cho, M. Chyu, Heat transfer in rotating channel with inclined pin-fins, J. Turbomach.-Trans. ASME 133 (2) (2011), 021003-1-021003-8.
[23] W. Yuan, J. Zhao, C.P. Tso, T. Wu, W. Liu, T. Ming, Numerical simulation of the thermal hydraulic performance of a plate pin fin heat sink, Appl. Therm. Eng. 48 (2012) 81–88.
[24] J. Zhao, S. Huang, L. Gong, Z. Huang, Numerical study and optimizing on micro square pin-fin heat sink for electronic cooling, Appl. Therm. Eng. 93 (2016) 1347–1359.
[25] B. Hollworth, L. Dagan, Arrays of impinging jets with spent fluid removal through vent holes on the target surface—Part 1: average heat transfer, J. Eng. Gas Turbines Power-Trans. ASME 102 (1980) 994–999.
[26] H.H. Cho, D.H. Rhee, Local heat/mass transfer measurement on the effusion plate in impingement/effusion cooling systems, J. Turbomach.-Trans. ASME 123 (2001) 601–608.
[27] E.Y. Choi, Y.D. Choi, W.S. Lee, J.T. Chung, J.S. Kwak, Heat transfer augmentation using a rib–dimple compound cooling technique, Appl. Therm. Eng. 51 (2013) 435–441.
[28] C. Wan, Y. Rao, P. Chen, Numerical predictions of jet impingement heat transfer on square pin-fin roughened plates, Appl. Therm. Eng. 80 (2015) 301–309.
[29] B. Han, R. Goldstein, Jet-impingement heat transfer in gas turbine systems, Ann. NY Acad. Sci. 934 (2001) 147–161.
[30] S.K. Hong, D.H. Lee, H.H. Cho, Effect of jet direction on heat/mass transfer of rotating impingement jet, Appl. Therm. Eng. 29 (2009) 2914–2920.
[31] K.M. Kim, H. Moon, J.S. Park, H.H. Cho, Optimal design of impinging jets in an impingement/effusion cooling system, Energy 66 (2014) 839–848.
[32] B.P. Whelan, A.J. Robinson, Nozzle geometry effects in liquid jet array impingement, Appl. Therm. Eng. 29 (2009) 2211–2221.
[33] P. Tie, Q. Li, Y. Xuan, Investigation on the submerged liquid jet arrays impingement cooling, Appl. Therm. Eng. 31 (2011) 2757–2763.
[34] B.P. Whelan, R. Kempers, A.J. Robinson, A liquid-based system for CPU cooling implementing a jet array impingement waterblock and a tube array remote heat exchanger, Appl. Therm. Eng. 39 (2012) 86–94.
[35] F. Monnoyer, D. Lochegnies, Heat transfer and flow characteristics of the cooling system of an industrial glass tempering unit, Appl. Therm. Eng. 28 (2008) 2167–2177.
[36] F. Cirillo, G.M. Isopi, Glass tempering heat transfer coefficient evaluation and air jets parameter optimization, Appl. Therm. Eng. 29 (2009) 1173–1179.
[37] S.-M. Lin, H.-F. Liu, W.-R. Wang, S.Y. Lee, C.-Y. Cheng, C.-Y. Li, Optimum design and heat transfer correlation equation of a mini radiator with jet impingement cooling, Appl. Therm. Eng. 89 (2015) 727–737.
[38] B. Wang, D. Lin, Q. Xie, Z. Wang, G. Wang, Heat transfer characteristics during jet impingement on a high-temperature plate surface, Appl. Therm. Eng. 100 (2016) 902–910.
[39] T. Ihli, R. Kruessmann, I. Ovchinnikov, P. Norajitra, V. Kuznetsov, R. Giniyatulin, An advanced He-cooled divertor concept: design, cooling technology, and thermohydraulic analyses with CFD, Fusion Eng. Des. 75–79 (2005) 371–375.
[40] P. Norajitra, R. Giniyatulin, T. Ihli, G. Janeschitz, P. Karditsas, W. Krauss, et al., European development of He-cooled divertors for fusion power plants, Nucl. Fusion 45 (2005) 1271.
[41] B. Končar, P. Norajitra, K. Oblak, Effect of nozzle sizes on jet impingement heat transfer in He-cooled divertor, Appl. Therm. Eng. 30 (2010) 697–705.
[42] B. Končar, I. Simonovski, M. Draksler, Influence of multiple jet cooling on the heat transfer and thermal stresses in DEMO divertor cooling finger, Fusion Eng. Des. 86 (2011) 167–173.
[43] B. Končar, M. Draksler, P. Norajitra, Design and cooling of the edge segments of the DEMO divertor target plates, Fusion Eng. Des. 88 (2013) 1831–1835.
[44] J. Rader, B. Mills, D. Sadowski, M. Yoda, S. Abdel-Khalik, Verification of thermal performance predictions of prototypical multi-jet impingement helium-cooled divertor module, Fusion Sci. Technol. 64 (2013) 282–287.
[45] M.S. Tillack, A.R. Raffray, X.R. Wang, S. Malang, S. Abdel-Khalik, M. Yoda, et al., Recent US activities on advanced He-cooled W-alloy divertor concepts for fusion power plants, Fusion Eng. Des. 86 (2011) 71–98.
[46] ANSYS CFX-Solver Theory Guide, ANSYS, 2013.
[47] N. Zuckerman, N. Lior, Jet impingement heat transfer: physics, correlations, and numerical modeling, Advances in Heat Transfer, Elsevier, 2006, pp. 565–631.
[48] B. Končar, M. Draksler, K. Oblak, P. Norajitra, V. Widak, Numerical investigation of multiple-jet cooling concept for helium cooled divertor, in: International Conference Nuclear Energy for New Europe, Portoroz, Slovenia, 2008.
[49] A. Gervash, R. Giniyatulin, A. Kokoulin, A. Komarov, V. Kuznetsov, A. Makhankov, Manufacturing and Testing the He-cooled Target Module Mock-ups for DEMO Fusion Reactor Divertor Tech. rep, EFREMOV Institute STC Sintez, St. Petersburg, 2006.
[50] Y.A. Çengel, A.J. Ghajar, Heat and Mass Transfer: Fundamentals & Applications, McGraw-Hill, 2011.
[51] L.F.G. Geers, Multiple Impinging Jet Arrays: An Experimental Study on Flow and Heat Transfer Ph. D. thesis, Thermal and Fluids Sciences, Delft University of Technology, Delft, The Netherlands, 2003.
[52] J. Brooks, Y. Cha, A. Hassanein, S. Majumdar, R. Mattas, D. Smith, Engineering Design of a Liquid Metal Cooled Self-Pumped Limiter for a Tokamak Reactor, Argonne National Lab, IL, USA, 1987.
[53] P. Norajitra, A. Gervash, R. Giniyatulin, T. Hirai, G. Janeschitz, W. Krauss, et al., Helium-cooled divertor for DEMO: manufacture and high heat flux tests of tungsten-based mock-ups, J. Nucl. Mater. 386–388 (2009) 813–816.
[54] J.M. Gere, Mechanics of Materials, THOMSON, 2006.
[55] B.S. Kim, B.S. Kwak, S. Shin, S. Lee, K.M. Kim, H.-I. Jung, et al., Optimization of microscale vortex generators in a microchannel using advanced response surface method, Int. J. Heat Mass Transfer 54 (2011) 118–125.
[56] K.M. Kim, H. Lee, B.S. Kim, S. Shin, D.H. Lee, H.H. Cho, Optimal design of angled rib turbulators in a cooling channel, Heat Mass Transfer 45 (2009) 1617–1625.
[57] D.G. Ullman, The Mechanical Design Process, McGraw-Hill, New York, 1992.